33RD CONGRESS
OF THE INTERNATIONAL COUNCIL
OF THE AERONAUTICAL SCIENCES
STOCKHOLM, SWEDEN, 4-9 SEPTEMBER, 2022

ICAS 2022 SWEDEN

# Effect of Nitriding on Microstructure and Mechanical Properties on a Ti64 Alloy for Aerospace Applications

S. Stekovic[1], R. Romero-Ramirez[1] and L. Selegård[2]

[1] Division of Engineering Materials, Linköping University, Linköping, Sweden
[2] Saab Aeronautics, Linköping, Sweden and Division of Molecular Surface Physics and Nanoscience, Linköping University, Linköping, Sweden

## Abstract

Titanium is 40% lighter than steel and is very strong in relation to its low weight, which makes it very interesting for lightweight applications. However, the use of titanium in certain aircraft components is limited because titanium is a relatively soft metal that quickly deteriorates when mechanically stressed. In this research, a nitriding heat treatment has been developed for Ti64 (Grade 5) alloy with the aim to improve wear properties without negative effect on fatigue and strength. The mechanical properties were studied through hardness and wear tests performed at room temperature in laboratory air on untreated and treated Ti64. Different measurements techniques were used to evaluate hardness on surface as well as polished cross-sections due to uncertainties in hardness measurements of thin films. The wear properties were investigated with pin-on-disc tests. The microstructures and nitrided surfaces were also investigated by optical microscopy, scanning electron microscopy (SEM) and surface profilometry. The analysis has shown that the nitriding process has led to the formation of an uneven compound layer and a diffusion zone beneath it. The energy dispersive X-ray spectroscopy (EDS) mapping showed a high concentration of nitrogen in the compound layer and aluminium in the diffusion zone. The microhardness measurements and nanoindentation have revealed the formation of an approximately 2.5 μm thick diffusion zone. The wear tests results showed a large difference in friction behaviour between the nitrided specimens, which has been associated with the failure of the nitrided layer and the wear rate.

**Keywords:** hardness, nanoindentation, nitriding, titanium, Ti64, wear

## 1. Introduction

Ti-6Al-4V (Ti64) is an alpha-beta titanium alloy commonly utilised in aerospace, automotive, chemical and maritime industries due to its high specific strength and excellent corrosion resistance. However, the use of Ti64 in some aircraft components is limited because it is a relatively “soft” metal that wears down quickly under mechanical stress. To improve hardness and consequently wear, different processes such as nitriding, carburising, plating, etc. are used. Nitriding is a thermo-chemical process that diffuse nitrogen (N) into surface of metals, and is used to improve surface properties, wear and corrosion resistance as well as fatigue strength of metal components [1]. After nitriding, a compound layer and an underlaying diffusion zone are formed near the surface. In the case of Ti64, the compound layer consists mainly of TiN and $Ti_2N$ titanium nitrides while the diffusion zone is composed of interstitial solid solution of nitrogen dissolved in the alloy [2]. The compound layer is not a traditional coating as it is grown together into the underlying Ti64 substrate.

The method is relevant today as it can potentially replace hard chromium plating which has been a standard industrial process for enhanced wear and corrosion protection in aerospace. Chromium

used in the hard chromium plating contains hexavalent chromium ($Cr^{6+}$) which is carcinogenic and toxic, and strongly controlled by the European Registration, Evaluation, Authorisation and Restriction of Chemicals (REACH) regulations [3]. Therefore, it is essential to find an alternative safer replacement to the hard chrome plating with similar or better properties and functions. There are several commercial alternatives available, for example High Velocity Oxygen Fuel (HVOF) spraying, and various physical and chemical vapour deposition processes, but they cannot fully replace hard chromium on their own [4, 5, 6, 7, 8]. Nitriding is a highly interesting alternative to hard chromium as it is environmentally sustainable and potentially can replace hard chromium in many applications.

The objective of this research has been to evaluate whether critical requirements for material and mechanical performance can be met with a new nitriding process on Ti64. This means that the nitrided Ti64 has been compared with untreated Ti64 through hardness indentations and sliding pin-on-disc wear performed at room temperature in laboratory air. Following the test procedure, the specimens were subjected to fractography and metallographic examinations by using light and electron scanning microscopy.

## 2. Materials and experimental methods

### 2.1 Materials

A commercially available annealed Ti64 alloy was used in two forms in the present study, i.e. as sheets made of ASTM B265-15 Gr.5 alloy with the chemical composition presented in Table 1 and as round bars made of ASTM 4928W alloy with the chemical composition presented in Table 2. The sheets were used for microstructure analysis and hardness measurements while the bars were used for mechanical testing as well as microstructural analysis before and after the tests.

Table 1 – Chemical composition of Ti64 sheets (%).

| | Fe | C | N | H | O | Al | V | Ti | Residual | |
|---|---|---|---|---|---|---|---|---|---|---|
| Requirement | ≤ 0.40 | ≤ 0.08 | ≤ 0.05 | ≤ 0.015 | ≤ 0.20 | 5.5-6.75 | 3.5-4.5 | Bal. | Each ≤ 0.10 | Total ≤ 0.40 |
| Analysis | 0.04 | 0.02 | 0.01 | 0.008 | 0.1 | 5.9 | 3.9 | Bal. | 0.1 | 0.4 |

The Rockwell hardness was measured to 35 HRC in the annealed round bars while for the sheets, the Rockwell hardness was 32 HRC.

Table 2 – Chemical composition of Ti64 bars (%).

| | Fe | C | N | H | O | Y | Al | V | Ti | Residual | |
|---|---|---|---|---|---|---|---|---|---|---|---|
| Requirement | max 0.30 | max 0.08 | max 0.05 | max 0.0125 | max 0.20 | max 0.005 | 5.5-6.75 | 3.5-4.5 | Bal. | Each ≤ 0.10 | Total ≤ 0.40 |
| Analysis | 0.17 | 0.021 | 0.017 | <0.0006 | 0.168 | <0.005 | 6.43 | 4.19 | Bal. | <0.1 | <0.4 |

The Ti64 material consists of two phases, namely, a main hexagonal close-packed (HCP) $\alpha$-phase and a second body-centered cubic (BCC) $\beta$-phase. Aluminium is added to stabilise the $\alpha$-phase while vanadium is the $\beta$-phase stabiliser. The properties of the $\alpha + \beta$ alloys can be controlled by heat treatment to produce a range of different mechanical properties [9, 10]. The maximum operating temperature is in the range of 315 to 400 $^{o}$C [11]. Nitriding process was performed on both sheets and bars, however, the detailed information about the process is not published at this time to protect the intellectual property rights.

## 2.2 Microstructural investigations

Specimens were examined using light optical microscopy (OP) and a HITACHI SU-70 field emission gun scanning electron microscopy (SEM) equipped with an energy dispersive X-ray spectroscopy (EDS) and electron backscatter diffraction (EBSD) from Oxford Instruments to determine microstructural features and damage. The specimens used for these observations were first sectioned using a diamond saw. After the sectioning, the specimens were mounted in Bakelite hot mounting resin with carbon filler, and ground on a rotating disc using SiC P320 grit and diamond suspension 9um. After grinding was completed, the specimens were polished using a silica oxide slurry 0,25um on a porous neoprene surface.

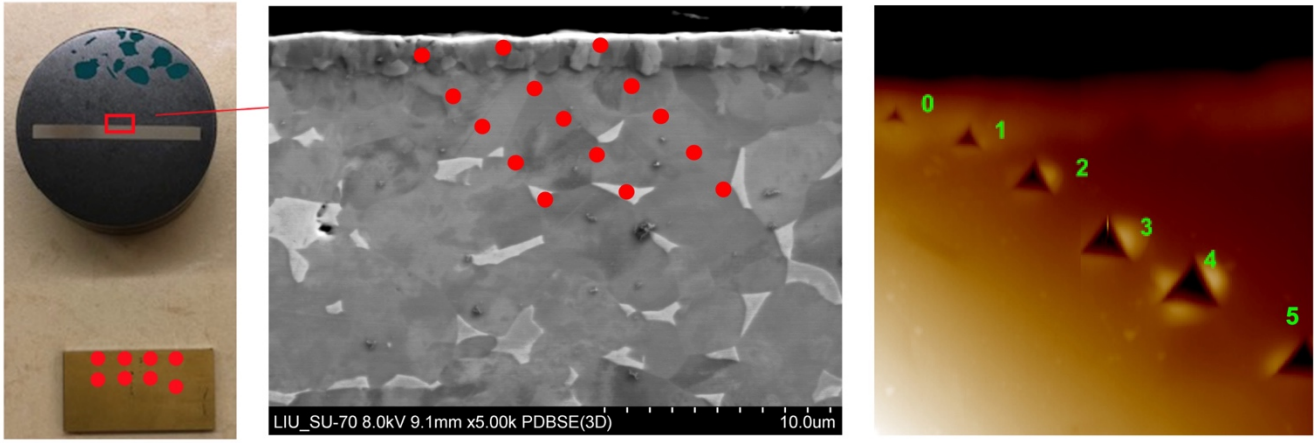


Figure 1 – Specimens for hardness measurements.

## 2.3 Hardness measurements

Hardness measurements were performed on nitrided specimens as shown in Figure 1. One specimen was in the form of a sheet (Figure 1, left image) for surface measurements while one was mounted in Bakelite and polished (Figure 1, middle and right image) for cross-section depth profiling. Three methods were used for the measurement of hardness due to the complexity of hardness measurements of thin films as well as to see if the measurements can be correlated. These methods include Vickers microhardness using Struers Durascan hardness test equipment and nanoindentation using Umis Nanoindenter from Fischer-Cripps labs and a NanoTest Vantage system with a diamond Berkovich indenter-tip from Micro Materials Ltd. The indenters have got a three-faced indenter with a similar face-to-depth ratio to the Vickers indenters and a tip that typically ranges between 50 to 100 nm in radius. Vickers microhardness measurements were carried out with different loads and the average hardness was obtained from five indentations for each load.

The nanoindentation measurements were load controlled using 4, 10, 12, 15 and 20 mN as the maximum load. Further, a fixed time was used for loading and 5 s for unloading with a dwell time at the maximum load of 5 s for the top surface measurements and 2 s for the cross-section measurements for the indentation measurements. At least 6 to 10 indentations were conducted for each type of measurement, and the average maximum depth, plastic depth, hardness, reduced modulus, elastic and plastic work were calculated from the measured values. The positions for the top surface measurements were randomly taken in a 3 x 3 grid, with 15 μm spacing between them. The cross-section measurements were done in specific locations in a single row along the nitrided layer as shown in Figure 1 on the left image. A separate measurement of the area below the nitrited layer was also performed in the cross-section (Figure 1, middle and right image).

## 2.4 Wear testing

Tribological characterisation under sliding wear conditions was performed on nitrided Ti64 tribopairs

as shown in Figure 2. In total, two pairs (two pins and two discs) were tested using a Phoenix tribology TE67 pin-on-disc friction and wear tester. The discs were flat with a diameter of 80 mm and a thickness of 8.4 mm while the pins were 30 mm long with a spherical radius of 3 mm at one end for the contact surface.

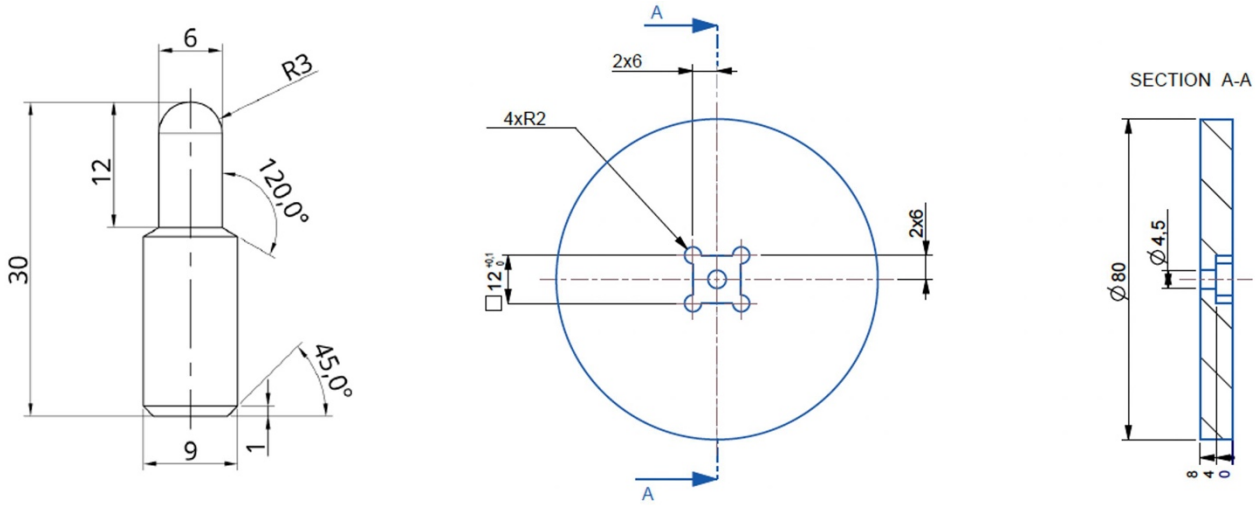


Figure 2 – Specimens used for wear testing.

Before the experiments, the pin samples were cut using Secotom-10 Precision Cutting Machine to remove a part of the pin with the 6 mm diameter to enable mounting of the sample in the tribometer as that originally the samples were machined for a different wear testing equipment. The tribological tests were carried out under unidirectional sliding conditions following the ASTM G99 standard procedure with a load of 4 N, a sliding speed of 0.2 m/s and a duration of 5 000 s at room temperature. The wear behaviour of the pin and disc specimens was evaluated using wear volume and wear rate. After the testing, the samples were rinsed with acetone, then cleaned with heptane in ultrasonic bath for 10 min and weighed using analytical scales. Wear volume was calculated by multiplying the average wear track profile area by the average track length. Further, optical Dino-Lite digital microscopy and Wyko 1100NT 3D optical profilometry analyses were conducted on the samples surfaces before the testing commenced, Figure 3. The coating on both disc samples had an oriented surface topography lay from the polishing process with multiple features among the surface, i.e. dark or light stripes or spots and several bigger stains. Multiple pores and short oriented scratches were also observed on the surface of disk 2/2. Pin 1/2 showed scratches in one direction with coating defects in the contact zone. Pin 2/2 showed some grey strains and chipped coating, which could have been possibly a deeper scratch.

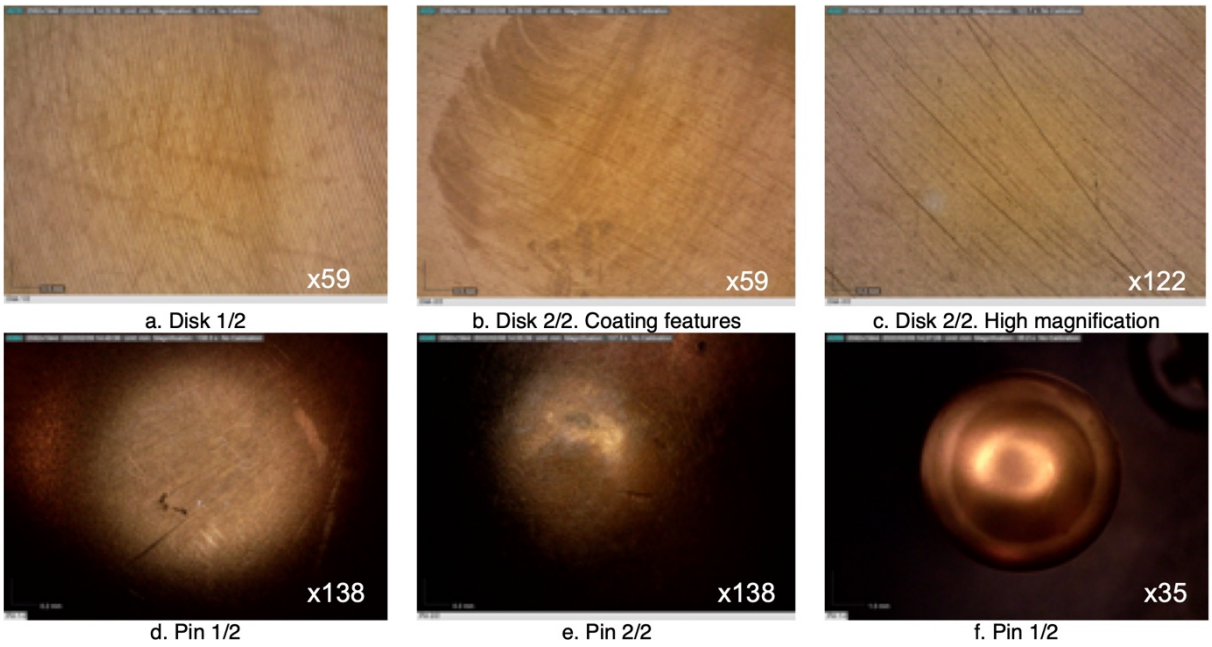


Figure 3 – Optical microscopy images (top images a-f) and surface roughness profiles (right image) of the sample surfaces before wear testing.

The roughness profiles and values are shown in Figure 4. It can be observed that Pin 1/2 has a lower Sa roughness (0.28 µm) compared to Pin 2/2 (0.97 µm). Similarly, Disc 1/2 has a Sa-values of 0.55 µm and Disc 2/2 has Sa of 0.24 µm.

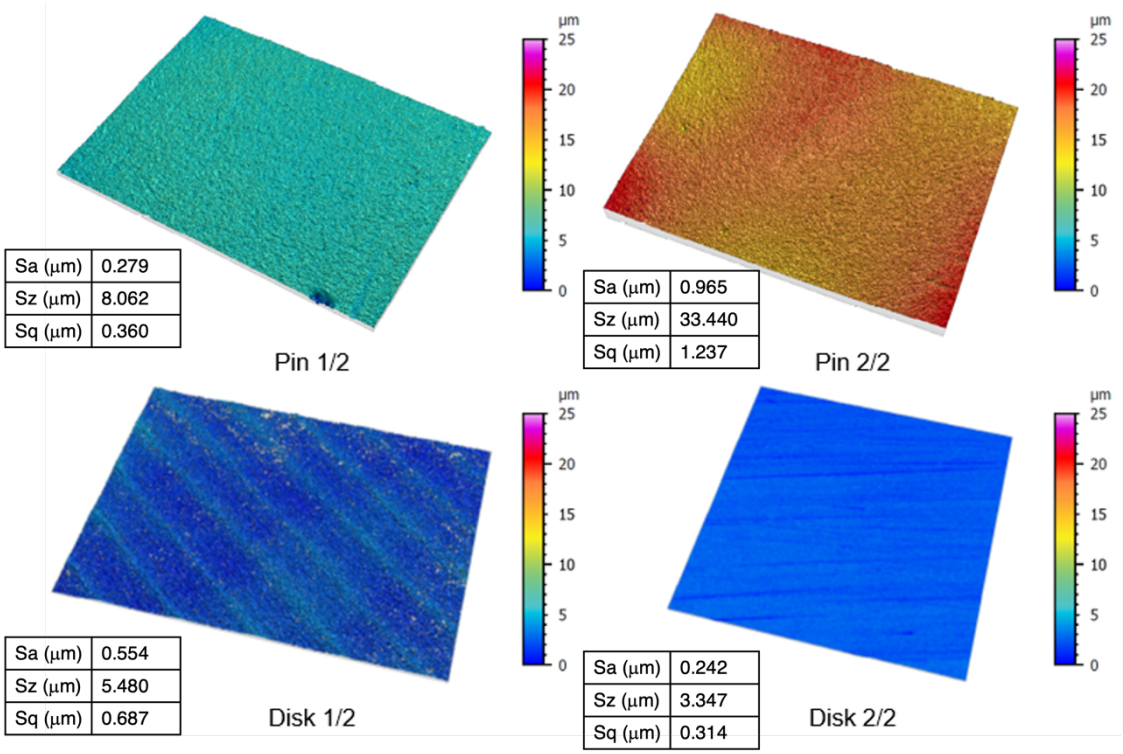


Figure 4 – Surface roughness profiles of the sample surfaces before wear testing.

## 3. Results and discussion

### 3.1 Initial microstructure

The samples for the analysis of the initial microstructure were taken from each side of a nitrided sheet specimen where one side had a deeper golden surface colour than the opposite side, Figure 5. The microstructure obtained after the nitriding process of Ti64 specimens consists of a titanium nitride compound layer clearly visible on the top area followed by a diffusion zone beneath the compound layer. The compound layer consists of two phases, TiN and $Ti_2N$, with a thickness that varies between 0.25 nm – 385 nm on the lighter golden side, and 1 μm – 1.69 μm on the deeper golden side. Likewise, the thickness of the diffusion layer was between 320 nm – 460 nm on the lighter golden side, and 0.8 μm – 2.5 μm on the deeper golden side. In the base Ti64-material, β-phase (the bright phase) was mostly observed in the grain boundaries. All hardness measurements were performed on the deeper golden side. Surface colours of the wear specimens were uniform with similar deeper golden hue.

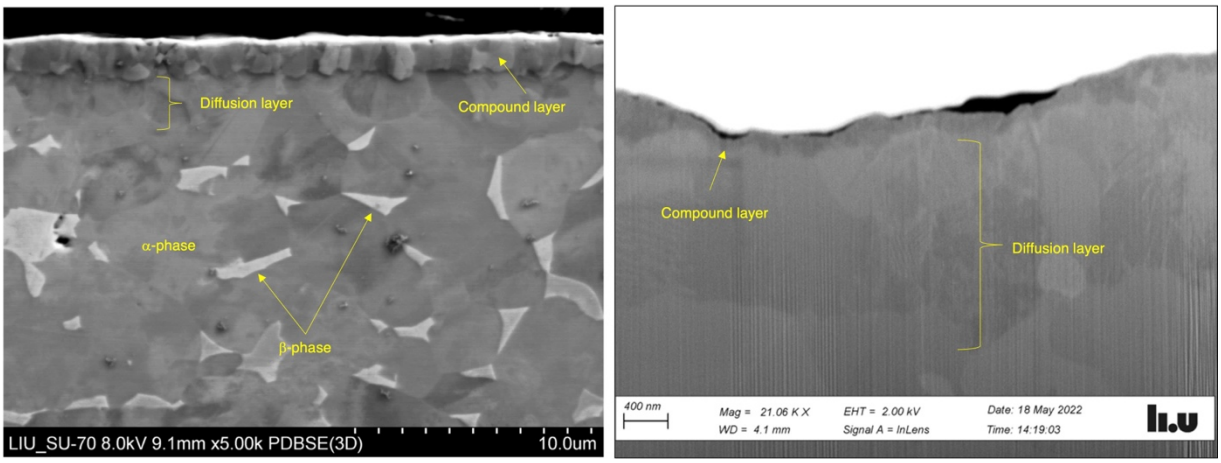


Figure 5 – Initial microstructures from two sides of a nitrided Ti-sheet at a lower (left image, deeper golden colour) and a higher magnification (right image, yellow-gold colour).

The EDS mapping of the effect of nitriding on Ti64 is presented in Figure 6. Highly concentrated nitrogen is observed at the compound layer while the diffusion layer is enriched in aluminium. Vanadium is concentrated in the β-phase precipitates.

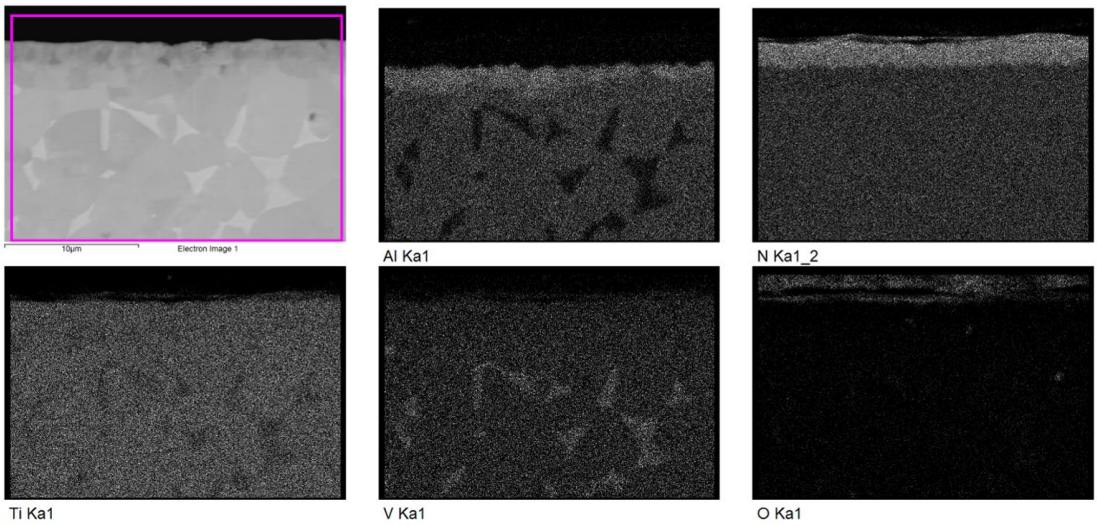


Figure 6 – EDS mapping on the cross-section of the nitrided sheet sample with deep golden colour.

The thickness non-uniformity of the compound and diffusion layer is probably due to the nitriding techniques performed at the sheet samples, for example, placement of the sample, nitrogen diffusion paths and directions into the substrate, distance to electrodes, etc.

## 3.2 Hardness measurements

The Vickers hardness values are presented in Table 3 where each value is average of five measurements. Vickers microhardness measurements were carried out with different loads and were taken from both the top surface and cross-sections. The obtained values for the top and diffusion layers are significantly lower than expected, which are in the range of 1 800 – 2 100 HV and 800 – 900 $HV_{0.1}$, respectively, [12]. The results show that the estimation of the real Vickers microhardness values of the nitrided layers was difficult due to the thickness of the layers, and effect from the surface finish and substrate. The indent depths are between 0.656 and 0.959 μm for HV 0.01, and 0.776 and 1.136 μm for HV 0.0025 when calculated as about $1/7^{th}$ of the diagonal length. However, as the thickness of the compound layer varies, the effect of the substrate cannot be neglected. Therefore, it was decided to use nanoindentation measurements in combination with two approaches from the literature to estimate Vickers hardness. The first approach was the geometrical approach suggested by Jönsson and Hogmark [13] while the second approach was based on the evaluation method from Kim et.al. [14].

Table 3 – Vickers hardness measurements.

| **Material** | **HV 0.01** | **HV 0.025** | **HV 0.05** | **HV 0.1** | **HV 1** |
|---|---|---|---|---|---|
| Top of the surface | 569 (St dev 181.18) | 1063 (St dev 189.54) | 557.33 (St dev 139.63) | 684.89 (St dev 80.86) | 402.2 (St dev 16,1) |
| Compound layer | NA | NA | NA | NA | NA |
| Diffusion layer | 558.67 (St dev 40.85) | 337 (St dev 68.66) | NA | NA | NA |
| Ti64 base material | NA | NA | NA | 321 (St dev 9.2) | 304.33 (St dev 2.1) |

The Jönsson and Hogmark approach calculates the composite hardness for Vickers indentation based on hardness measurements of the coating and substrate by using weighted law of mixture. They have considered two limit cases, namely, when the film is plastically strained to match the indenter tip on harder substrate and when a hard brittle film cracks on softer substrate. Both cases require information about the film thickness, composite hardness and substrate hardness measured with the same constant indentation size, and diagonal indentation length obtained from SEM analysis. With the parameters values of the two case models from [13], the measured HV1 hardness of the composite and substrate from Table 3, a total film thickness of 4.29 μm including the diffusion layer and a diagonal indentation length of 67.92 μm, the Vickers hardness of the compound layer was estimated to 1118 HV using the limit case 1 model (plastically strained thin film) and 1849 HV using the limit case 2 model (brittle film on a soft substrate) when applying 1 kgf. The cracks were clearly visible in the vicinity of the indentation at the top layer, Figure 7 and 8, affecting accuracy of the measurements. With a load of 0.1 kgf and the measured indentation length of 24 μm, the Vickers hardness was calculated to values of 1457 HV and 2413 HV for the case 1 and 2, respectively. The indentations with HV1 and HV 0.1 on the top layer as well as the substrate are shown on both Figure 7 and 8. The HV0.1 indent was barely visible on the top layer after the test due to the toughness of the nitrided layer and the surface roughness effects. There were also bulges observed at the outer contour of the HV0.1 indent in the substrate (Figure 7, right image).

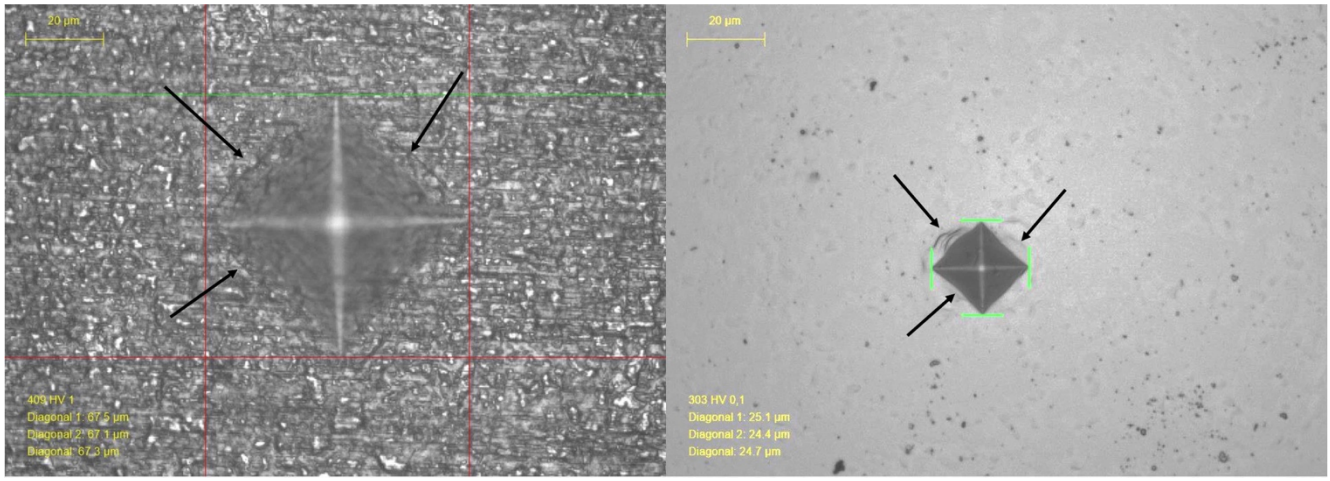


Figure 7 – Optical microscopy images of the indentation produced at the top layer (HV1, left image) and the substrate (HV0.1, right image).

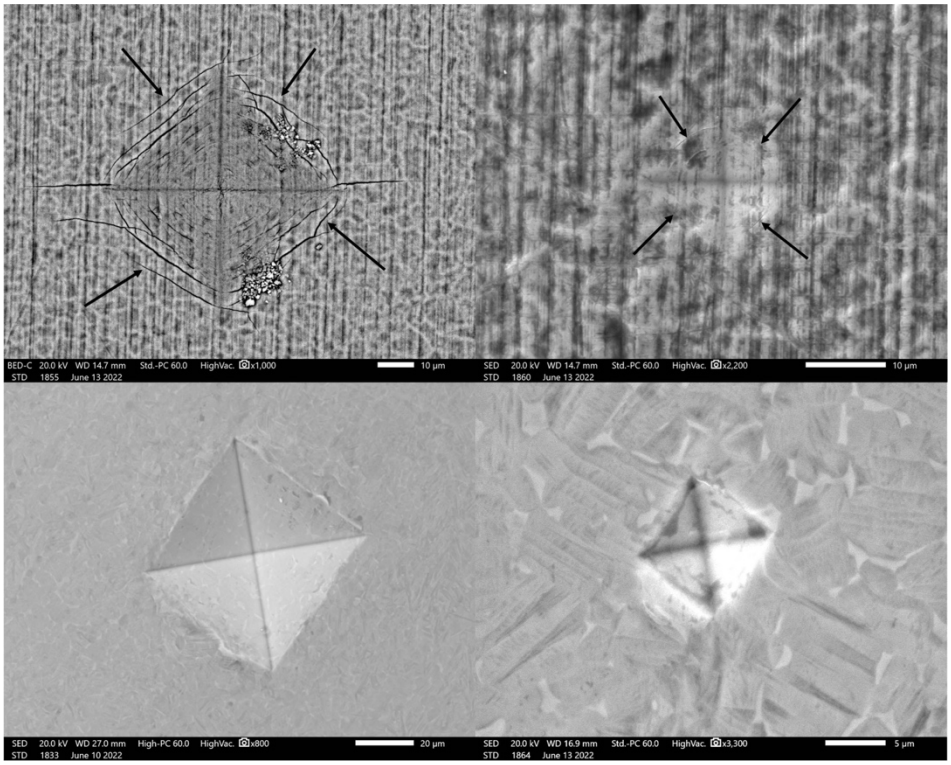

Figure 8 – SEM images of the indentations produced at the top layer (top row) and the substrate (bottom row). Loads were HV1 (left image) and HV0.1 (right image).

Nanoindentation tests were performed at same specimens shown in Figure 1 but on different locations to avoid effect from the Vickers indentations. The measurements were then used to calculate Vickers hardness based on [15], Table 4. For comparison, additional nanoindentation measurements were performed at another laboratory. The hysteresis curves from all the indentation positions are shown in Figure 9 on the left while the resulting calculated properties are shown in Table 5. It can be observed that the nitriding process leads to higher hardness close to the surface but also to a softer substrate. Further, the process results in a deeper nitriding depth with a clear change in the hardness profile.

Table 4 – Calculated Vickers hardness based on work from [15].

| Point | H_n (GPa) | H_V (kg/mm^2) |
|---|---|---|
| 0 | 24.64 | 2 328 |
| 1 | 26.86 | 2 539 |
| 2 | 18.20 | 1 720 |
| 3 | 11.65 | 1 101 |
| 4 | 7.43 | 702 |
| 5 | 5.80 | 549 |
| 6 | 6.73 | 636 |

** Note that the measurements points are shown in Figure 1.*

The top surface measurements showed high scatter from indent to indent, as clearly seen in the hysteresis curves and as represented by the high standard deviation in Table 5. This scatter is largely associated to the high surface roughness of the specimen and due to the low load used for the experiment. The step observed during the unloading part of the curve at around 0.3 mN is related to a thermal drift correction done as part of the measurement to account for variations in depth due to thermal effects. It is important to note that the maximum penetration depth was 102 nm and the coating thickness estimated to be between 1 µm – 1.7 µm, which means that only small influences from the substrate were expected.

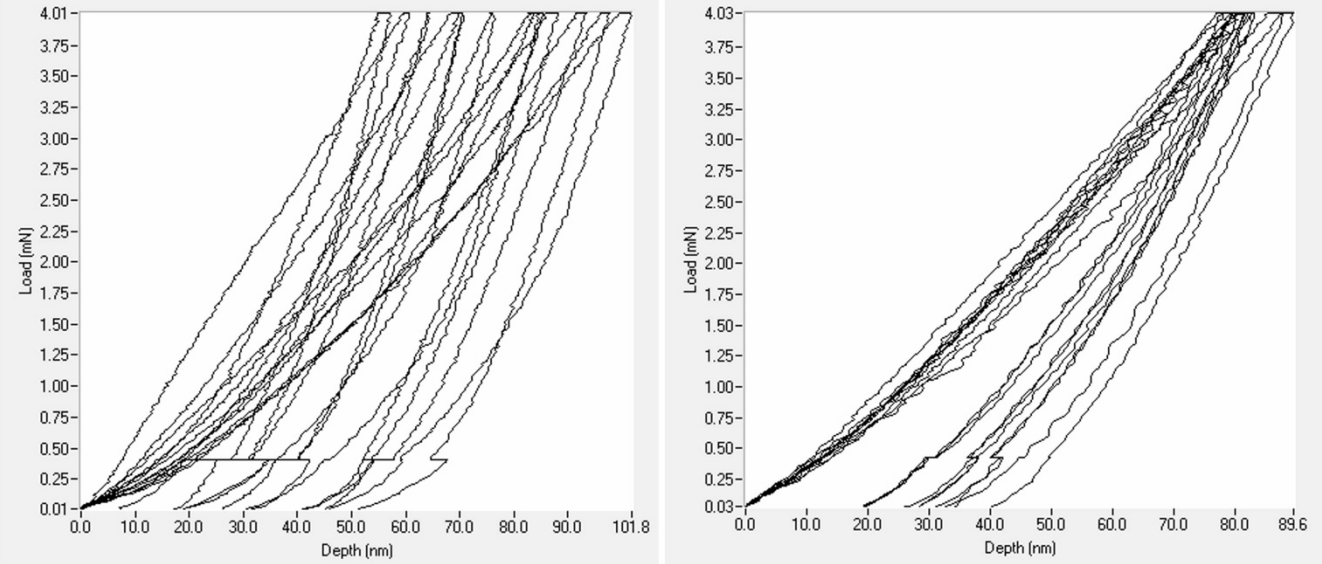


Figure 9 – Load vs depth hysteresis curves from all top surface (left) and all cross-sections (right) indentations.

The cross-section measurements were difficult to measure due to the thickness of the coating and the uncertainties regarding the exact positioning of the indents using the optical microscope (maximum magnification 40X). Since the nitrided layer is a thin film, and the positioning using the microscope has an approximate lateral resolution of ±1 µm, it was difficult to be certain where the tip would make contact with the sample. Furthermore, the cross-sections have a natural curvature towards the edge, which is generated during the sample preparation, and this curvature can cause slip of the indenter as the measurement is performed. In addition to this, the material can also collapse due to lack of support leading to uneven loading and unloading.

Table 5 – Calculated properties from the top surface and cross-section load-depth curves.

| **Property (top)** | **Average value** | **Std. Dev.** | **Property (cross-sections)** | **Average value** | **Std. Dev.** |
|---|---|---|---|---|---|
| Hardness (GPa) | 20.81 | 7.41 | Hardness (GPa) | 24.53 | 2.57 |
| Reduced modulus (GPa) | 314.38 | 84.85 | Reduced modulus (GPa) | 245.60 | 10.55 |
| Max depth (nm) | 79.25 | 14.77 | Max depth (nm) | 82.73 | 3.57 |
| Plastic depth (nm) | 60.29 | 13.72 | Plastic depth (nm) | 56.73 | 4.10 |
| Elastic work (nJ) | 0.067 | 0.008 | Elastic work (nJ) | 0.090 | 0.005 |
| Plastic work (nJ) | 0.064 | 0.025 | Plastic work (nJ) | 0.062 | 0.012 |

Figure 9 on the right shows the hysteresis curves from the cross-section measurements with the calculated mechanical properties presented in Table 5. It can be concluded from these results that less scatter was obtained in the measurements from indent to indent compared to the top surface measurements. The calculated hardness in this case was 24.5 GPa, which was slightly higher compared to the top surface, but the reduced modulus was 245 GPa, which was almost 70 GPa lower than the top surface measurement. Additionally, the elastic work was also higher in the cross-section measurements (0.09 nJ compared to 0.07 nJ) but the plastic work was similar in both cases. In the case of depth penetration, both measurements yielded similar results. For reference, the substrate hardness was also measured at 4 mN. A hardness of 5.5 $\pm$ 0.75 GPa and a reduced modulus of 144 $\pm$ 12 GPa were obtained. It is important to point out that even though better reproducibility was observed for the measurements in the cross-section, there is an uncertainty of whether there was slip of the indenter tip during the measurement, as no indentation imprint could be confirmed after the indentation procedure. However, the load vs. depth curves are homogeneous, so it is likely that the indentation was stable.

The curvature and the slip of an indentation are shown in Figure 10. The indentation was performed at high load of 50 mN to evaluate the exact position of the coating within the surface by 3D mapping. The 3D map is obtained by scanning the indenter tip against the sample at low loads. With this map, the location of the indentations can be more accurately selected compared to the optical microscopy as the locations are based on coordinates within the scan.

Figure 11 shows the surface map used to define the indent locations, and the appearance of the surface itself before and after the measurements. As it can be seen in Figure 11a, the indentations were done exactly at the first contour, which is where the cross-section transitions into the surface and where the thin film is expected. Figures 11b and 11c show the map before and after the scan. No remaining indent imprints could be detected after the measurements as a result of the combined effect of the very shallow marks (low load and high hardness) and the resolution used for the scan.

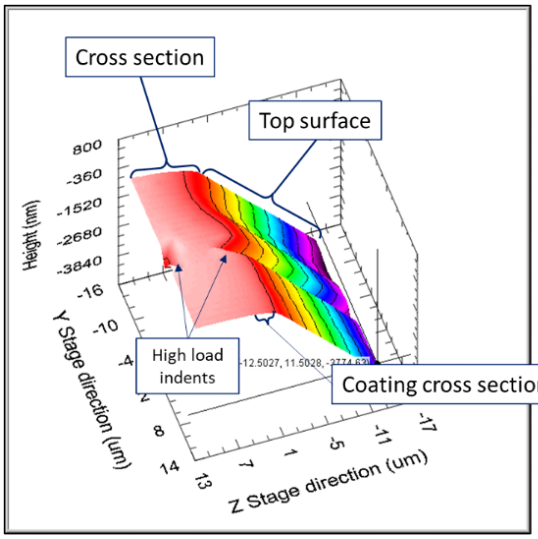


Figure 10 – 3D map highlighting the presence of curvature near the edge of the cross-section and the slip caused during indentation.

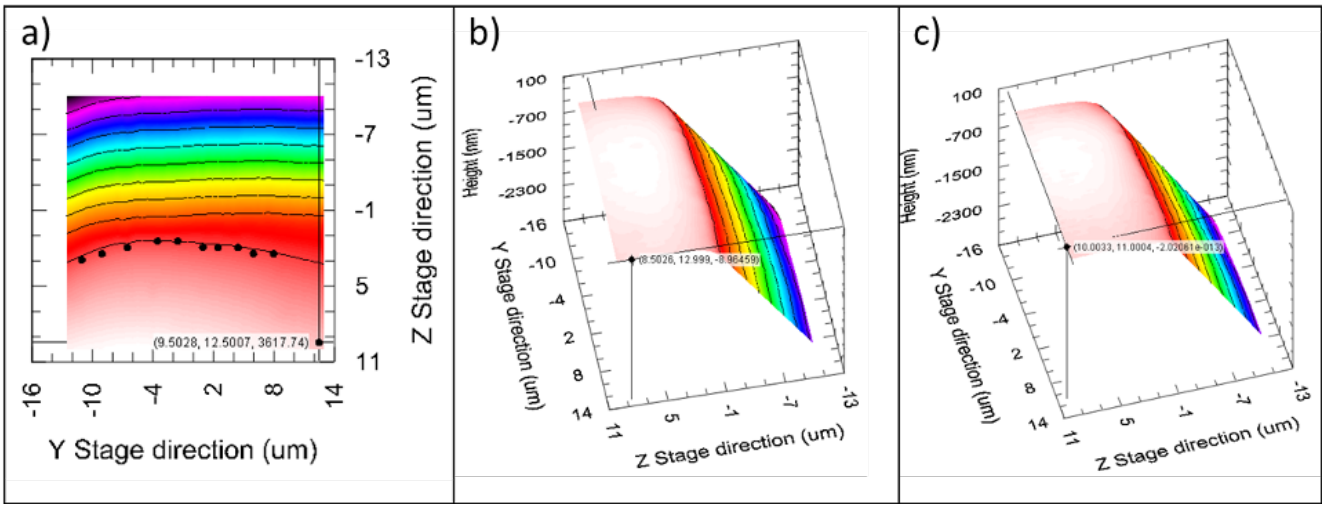


Figure 11 – 3D map of the surface used for indentation: a) location of the indentations performed, b) surface before indentations and c) surface after indentation.

## 3.3 Wear properties

The dependence of the coefficient of friction (COF) on time is shown in Figure 12, left image. As observed, the initial friction behaviour is very different between the two tests. The tests involving Pin 1/2 and Disc 1/2 shows an initial low friction that increases very abrupt and then stabilises at 0.5. In contrast, the test with Pin 2/2 and Disc 2/2 shows a very high initial friction, which gradually reduces and then stabilizes close to 0.5 after nearly 3600 s.

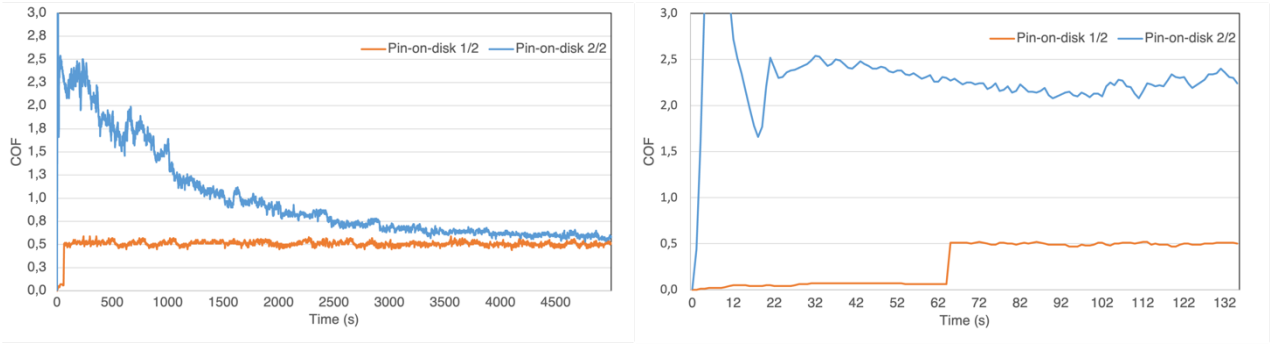


Figure 12 – Friction as a function of time for the two tests (left image) and initial friction as a function of time (right image).

The large difference in friction is associated to failure of the nitrided layer. In the case of testing the friction pair pin-on-disk 1/2, failure of the coating occurs after about 60 s (Figure 12, right image) of the experiment, which corresponds to the acceleration of the rig to the stabilisation of the rotation speed at 0.2 m/s. In the second pin-on-disc 2/2 test, the coating also failed in the beginning of the test (visual observation), but the friction coefficient curve differs significantly from the first test. Based on the high coefficient of friction and its significant fluctuations at the beginning of this test, significant ploughing friction was occurring (Figure 12). One reason for this is the exposure of the soft Ti64 substrate on the disc when the nitrided layer fails while the nitrided layer (and shape) of the pin is more or less intact. This results in deformation and ploughing by the pin into the disc.

The results of the wear measurements are presented in Table 6 and in Figure 13.

Table 6 – Wear volumes, weight loss and wear scar dimensions.

| **Sample** | **Weight loss (mg)** | **Wear scar diameter (mm)** | **Wear volume ($mm^3$)** | **Wear scar width (mm)** |
|---|---|---|---|---|
| Pin 1/2 | 2.99 | 2.655 | - | - |
| Pin 2/2 | 4.35 | 2.784 | - | - |
| Disc 1/2 | - | - | 8.74 | 2.100 |
| Disc 2/2 | - | - | 12.44 | 2.397 |

The wear rate of specimens 1/2 are lower compared to samples 2/2. This also correlates to the observed friction behaviour where high and unstable friction was seen for the test with pin and disc 2/2.

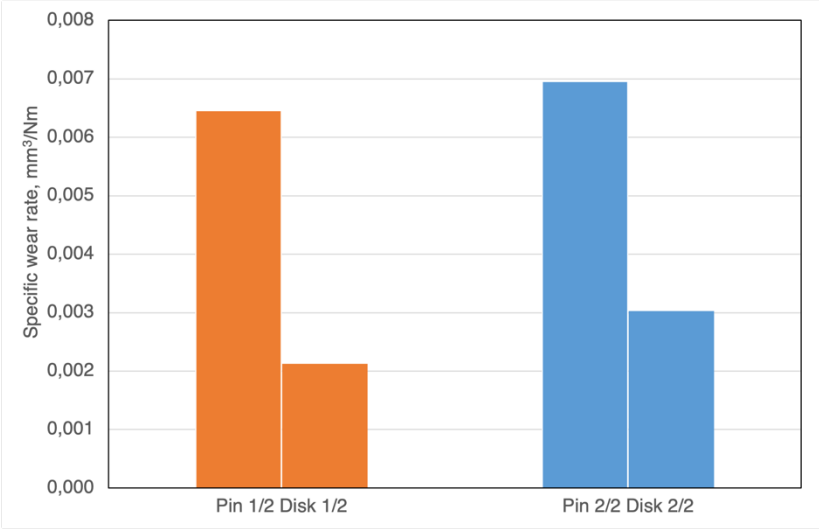


Figure 13 – Specific wear rate values.

The worn surfaces of the pins are shown Figure 14. The wear scars show very similar features despite the difference in the wear rate. This is somewhat expected since the friction levels at the end of both tests are similar which indicates that the interfacial mechanisms should be similar. Similarly, the worn surfaces of the disc specimens are shown in Figure 15. These are also similar to each other as well as to the pins. Since the contact at the end of the test is self-mated Ti64 it is also expected to see similar wear mechanisms on both interacting surfaces.

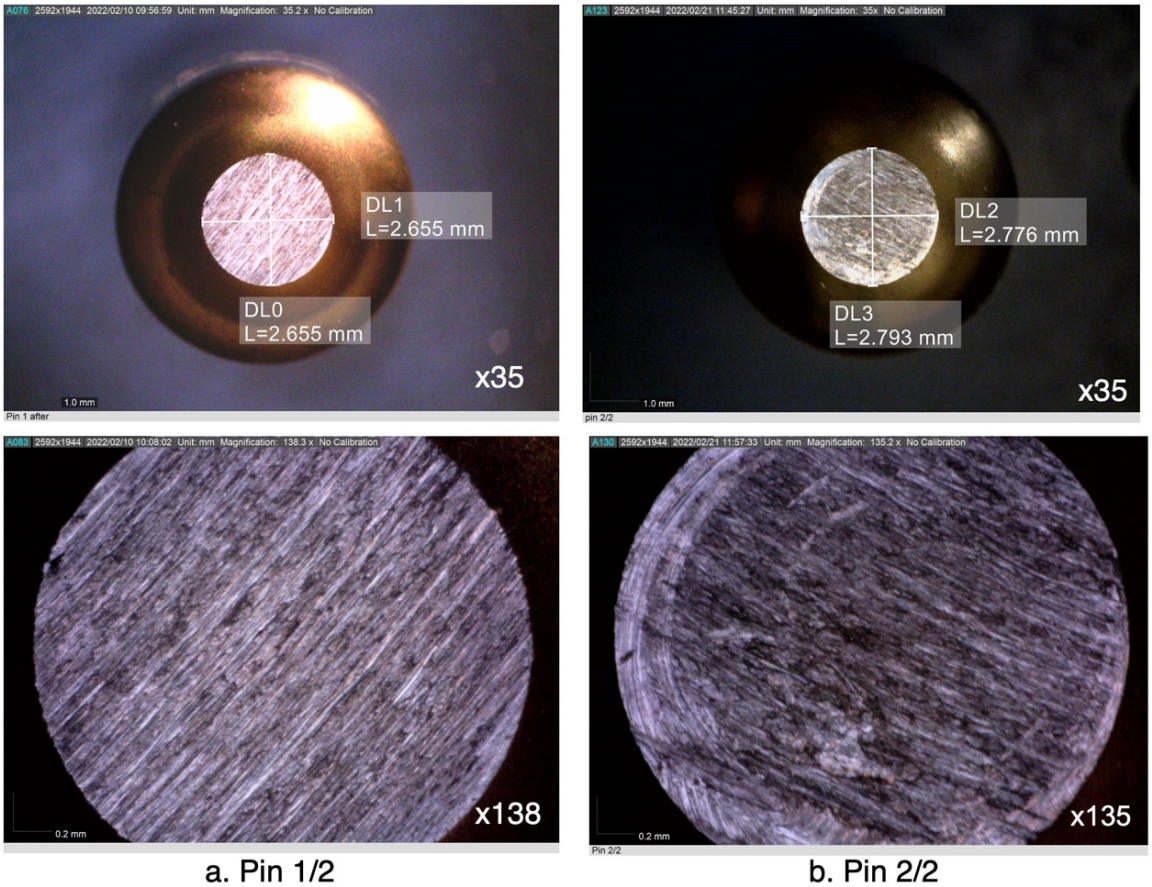


a. Pin 1/2 b. Pin 2/2

Figure 14 – Worn surfaces of the pins after tribological testing.

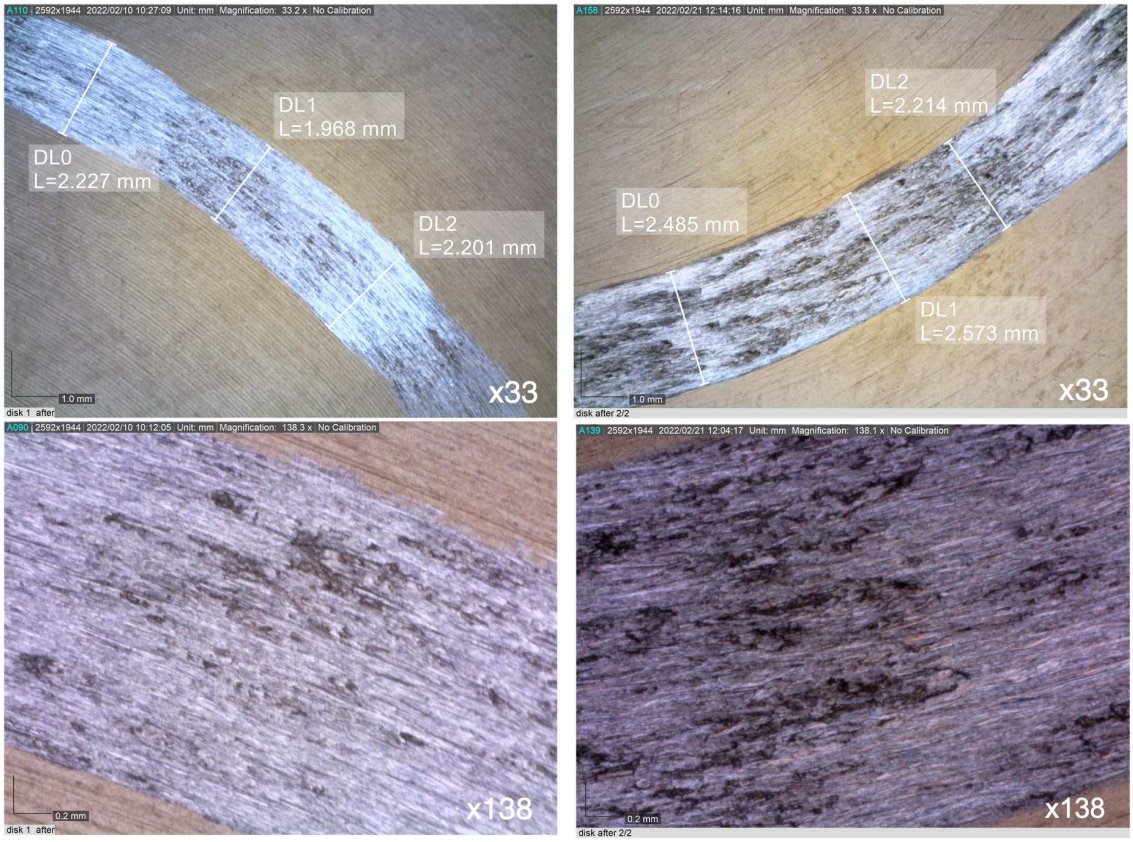


a. Disc 1/2 b. Disc 2/2

Figure 15 – Worn surfaces of the discs after tribological testing.

In Figure 16, the wear scar profiles on both disc specimens can be seen. The uneven topography in the wear track correlate with the features seen in Figure 15 and indicate mainly adhesive wear.

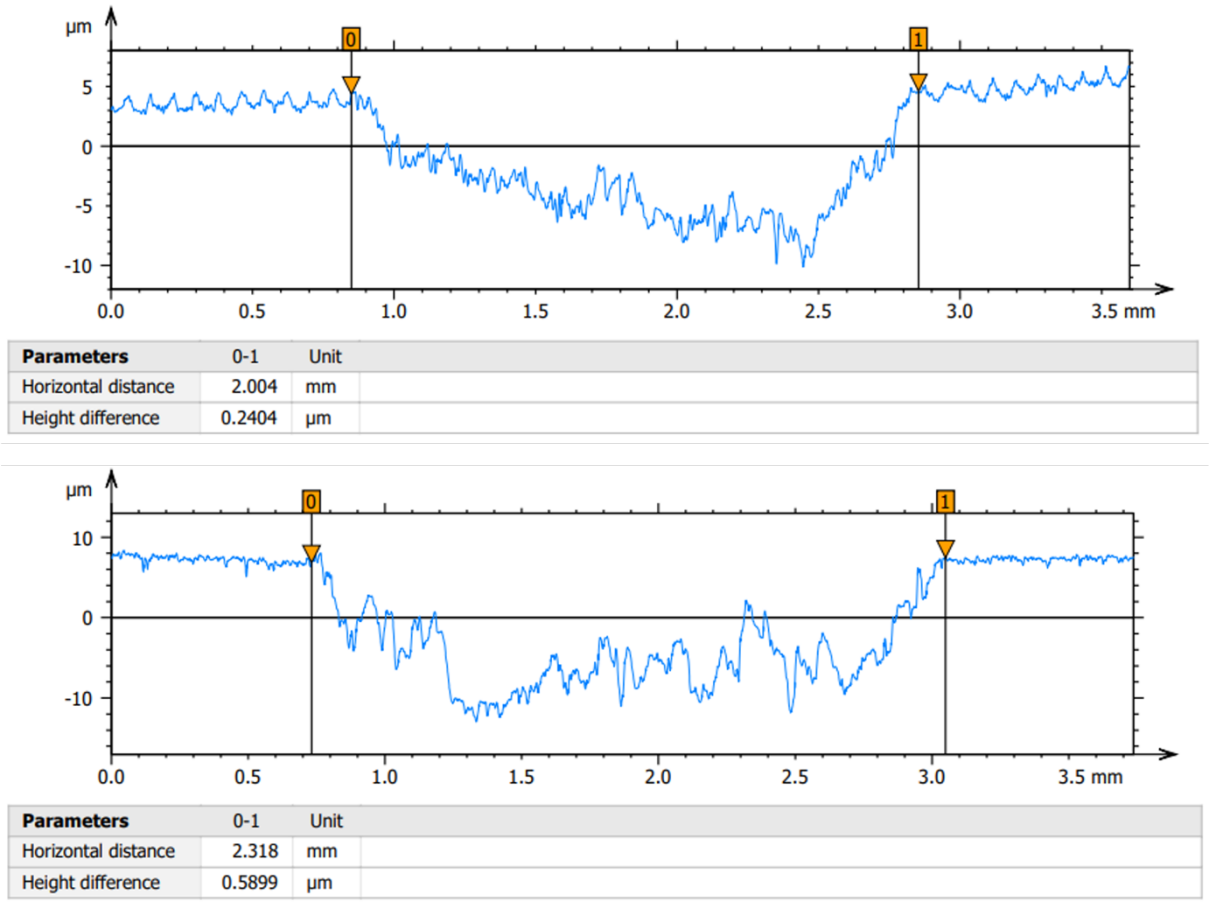


| Parameters | 0-1 | Unit |
|---|---|---|
| Horizontal distance | 2.004 | mm |
| Height difference | 0.2404 | µm |




| Parameters | 0-1 | Unit |
|---|---|---|
| Horizontal distance | 2.318 | mm |
| Height difference | 0.5899 | µm |

Figure 16 – Wear scar profiles on the discs after testing (a) disc 1/2 and (b) disc 2/2.

## 4. Conclusions

Hardness and tribological tests were performed to evaluate mechanical properties of a nitrided process on Ti64 Grade 5 alloy. The findings from the study are as follows:

- The nitriding process results in a thin compound layer and a thicker diffusion zone beneath the compound top layer. The overall nitriding process needs to be optimised to homogenise thickness of the compound layer as it influences the mechanical properties and it seems that the Ti64 samples did not receive an optimal nitriding heat treatment.

- The hardness measurements of the compound layer are not easy to perform and interpret because the hardness is affected by deformation of the compound layer, surface roughness and substrate itself.

- The mechanical properties of the compound layer vary depending on the type of measurement as higher hardness, lower reduced modulus and higher energy work were observed in the cross-sections, however, the penetration depth and plastic work were similar.

- Top surface measurements were significantly affected by the surface roughness of the nitrided layer leading to scatter due to interaction between surface asperities and the indenter tip. Cross-section measurements can be affected by the curvature at the edge of the nitrided layer. Further, uncertainties remain as no print is observable after the indentation.

- The two identical tribo pairs show very different friction behaviour. Initial friction with intact nitride layer on both surfaces results in low friction. The steady-state friction of self-mated Ti64 (without the nitrided layers) is ~ 0.5.

- The nitrided layer has limited adhesion to the substrate under dry friction conditions. In both performed tests, the nitrided layer on the disc fractures and is removed during the first seconds of the test. The wear scar features are very similar on both pin and disc surfaces and indicate mainly adhesive wear.

**Acknowledgments:** This project has received funding from the SIP LIGHTer, a strategic innovation programme (SIP) focusing on lightweight solutions under agreement 2018-02830.

## References

[1] www.bodycote.com

[2] Perez P. Influence of nitriding on the oxidation behaviour of titanium alloys at 700 ºC. *Surface and Coating Technology,* Vol. 191, Issues 2-3, pp 293-302, 2005.

[3] https://eur-lex.europa.eu/legal-content/EN/TXT/?uri=CELEX:32006R1907.

[4] Kubinski JA, Hurkman T, Trinh T, Fleischer W and van der Kolk. Perspective for Replacement of Hard Chromium by PVD. *Plating & Surface Finishing*, The Surface Technology Environmental Resource Center, 1999.

[5] Bryskin B, Kostylev A, Pokrovskiy Y and Lumpov A. CVD Technology for Preparing Wear-Resistive Chromium Carbide Coatings of Engine Components. *SAE International Journal of Materials and Manufacturing*, *7*(3), 630–632, 2014.

[6] Zhuk, Y. CVD Coating to Replace Hard Chrome Plating on Internal Surfaces and Complex Shaped Parts, *Aeromat 22 Conference and Exposition American Society for Metals*, 2011.

[7] Zhuk, Y. CHEMICAL VAPOR DEPOSITION COATINGS EXTEND AEROSPACE COMPONENT LIFE: Nanostructured tungsten-tungsten carbide chemical vapor deposition (CVD) coatings provide a practical, technical, and commercially viable alternative to hard chrome plating for aircraft components. *Advanced Materials & Processes*, vol. 175, no. 6, pp. 23+, 2017.

[8] Yang Z. Alternatives to hard chromium plating on piston roads. Degree Project of 30 credit points, Master of Science in Engineering, Mechanical Engineering, Karlstads University, 2011.

[9] Pedersen R. Microstructure and Phase Transformation of Ti-64-4V. *Licentiate Thesis.* Luleå University of Technology, 2002.

[10] Lütjering G. Influence of processing on microstructure and mechanical properties of (a + b) titanium alloys. *Materials Science and Engineering A243*, pp 32-45, 1998.

[11] Boyer R.R. An overview on the use of titanium in the aerospace industry. *Materials Science and Engineering: A*, Vol. 213, Issues 1–2, pp 103-114, 1996.

[12] https://www.ahtcorp.com/articles/blog/plasma-ion-nitriding-of-titanium-alloy-products-for-enhancing-their-tribological-and-anticorrosion-properties/

[13] Jönsson B and Hogmark S. Hardness Measurements of Thin Films. *Thin Solid Films*, pp257-269, 1984.

[14] Kim J-H, Tabaru T and Hirai H. Evaluation Technique of the Hardness and Elastic Modulus of Materials with Fine Microstructures. Materials Transactions, 44(4), 673-676, 2003.

[15] Lu Y, Su Y, Ge W, Yang T, Yan Z, Wang Y and Xia S. Conversion between Vickers hardness and nanohardness by correcting projected area with sink-in and pile-up effects. *Plasma Science Technology 22*, 065602, 2020.

### Copyright Statement